THESIS FOR THE DEGREE OF LICENTIATE OF ENGINEERING

Thermoelectric plastics: Structure-property relationships of P3HT

JONNA HYNYNEN

CHALMERS

Department of Chemistry and Chemical Engineering
Division of Applied Chemistry
CHALMERS UNIVERSITY OF TECHNOLOGY
Gothenburg, Sweden, 2018

Thermoelectric plastics: Structure-property relationships of P3HT

JONNA HYNYNEN

Thesis for the Degree of Licentiate of Engineering

Nr. 2018:02

Department of Chemistry and Chemical Engineering
Division of Applied Chemistry
Chalmers University of Technology
SE-41296 Gothenburg

Phone: +46 (0)31 772 1000

Cover:
Illustration of *Internet of Things*, prospective potentials to connect multiple small devices using plastic thermoelectrics.
Illustration by Mattias Larson

Chalmers Reproservice

Gothenburg, Sweden 2018

Thermoelectric plastics: Structure-property relationships of P3HT

Jonna Hynynen

Department of Chemistry and Chemical Engineering

Chalmers University of Technology

ABSTRACT

The advancing development of inter-connected small devices, so-called *Internet of Things* is increasing the demand for independent power sources. Heat is an abundant and often wasted source of energy, thermoelectric generators could be used to harvest this waste energy. Small devices such as heart-rate monitors or gas sensors *etc*. could potentially be powered by the heat dissipated from the human body using flexible plastic thermoelectric generators.

This thesis discusses thermoelectric plastics and in particular the semiconducting polymer P3HT. P3HT is a model conjugated polymer that is commercially available and has become an important reference material for the study of optoelectronic processes in organic semiconductors.

At first, we investigated doping from the vapor phase, which permits us to disentangle the influence of polymer processing and doping. We demonstrate that improving the degree of solid-state order of P3HT strongly increased the electrical conductivity.

Secondly we studied how the increased solid-state order of P3HT influenced the Seebeck coefficient and the power factor of vapor doped P3HT. Overall, the Seebeck coefficient did not vary to a larger extent whilst the power factor increased by one order of magnitude, to a value of about 3 $\mu W\ m^{-1}\ K^{-2}$. This increase was attributed to the improved mobility of charge carriers in the more ordered P3HT.

Keywords: Thermoelectric plastic, vapor doping, P3HT, F4TCNQ, structure-property relationships

NOMENCLATURE

CB	Chlorobenzene
CF	Chloroform
DDQ	2,3-dichloro-5,6-dicyano-*p*-benzoquinone
EU	European Union
F2TCNQ	2,5-difluoro-7,7,8,8-tetracyanoquionodimethane
F4TCNQ	2,3,5,6-tetrafluoro-7,7,8,8-tetracyanoquinodimethane
FTS	(Tridecaflouro-1,1,2,2-tetrahydrooctyl)trichlorosilane
GHG	Greenhouse Gas Emissions
GIWAXS	Grazing-Incident Wide-Angle X-ray Scattering
HOMO	Highest Occupied Molecular Orbital
IoT	Internet of Things
M_n	Number average molecular weight
M_w	Weight average molecular weight
LUMO	Lowest Unoccupied Molecular Orbital
oDCB	*o*-dichlorobenzene
P3HT	Poly(3-hexylthiophene)
P3HTT	Poly(3-hexylthiothiophene)
PBTTT	Poly(2,5-bis(3-tetradecylthiophen-2-yl)thieno[3,2-*b*]thiophene)
PEO	Poly(ethylene oxide)
PF	Power Factor
rr	Regioregularity
TCB	1,2,4-trichlorobenzene
TEG	Thermoelectric Generator
TFSI	Fe(III)triflate
TGA	Thermogravimetric Analysis
UV-vis-NIR	Ultraviolet-visible-near-infrared
ZT	Figure of Merit

PUBLICATIONS

This thesis consists of an extended summary of the following appended papers:

Paper I **Enhanced Electrical Conductivity of Molecularly p-Doped Poly(3-hexylthiophene) through Understanding the Correlation with Solid-State Order**
Jonna Hynynen, David Kiefer, Liyang Yu, Renee Kroon, Rahim Munir, Aram Amassian, Martijn Kemerink and Christian Müller
Macromolecules, 2017, **50**, 8140

Paper II **Influence of crystallinity on the thermoelectric power factor of P3HT vapour-doped with F4TCNQ**
Jonna Hynynen, David Kiefer and Christian Müller
RSC Advances, 2018, **8**, 1593-1599

The author has published the following papers which are not included in the thesis:

Thermoelectric plastics: from design to synthesis, processing and structure-property relationships
Renee Kroon, Desalegn Alemu Mengistie, David Kiefer, Jonna Hynynen, Jason D. Ryan, Liyang Yu and Christian Müller
Chemical Society Reviews, 2016, **45**, 6147

Bulk Doping of Millimeter-Thick Conjugated Polymer Foams for Plastic Thermoelectrics
Renee Kroon, Jason D. Ryan, David Kiefer, Liyang Yu, Jonna Hynynen, Eva Olsson and Christian Müller
Advanced Functional Materials, 2017, **27**, 1704183

CONTRIBUTION REPORT

Paper I The experimental design and preparation of samples. The electrical testing as well as optical and GIWAXS measurements and evaluation. Written parts of the paper.

Paper II The preparation of samples. The measurement of the electrical properties as well as the optical and Seebeck measurements and evaluation. Written a significant part of the paper.

TABLE OF CONTENT

Chapter 1

INTRODUCTION

1.1 Global Energy Production

The carbon dioxide levels have risen rapidly since the beginning of the industrial age leading to a change in the global climate. The European Union (EU) has set its goal on reducing greenhouse gas emissions (GHG) by 80-95 % by 2050, compared to the emissions levels in 1990 (Figure 1). Key energy-policy areas must not only revolve around the adaption of green energy sources (e.g. wind, solar and hydro power) but also seek to improve the energy efficiency of a society.

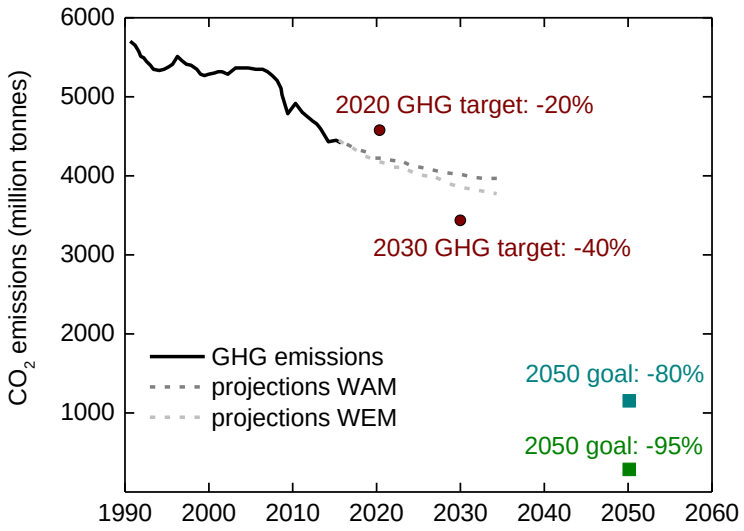

Figure 1. GHG emission, projections, target and goal for 2050. Projections are made 2017 "with existing measures" (WEM) taking into consideration existing polices and "with additional measures" (WAM) taking into consideration planned actions reported by member states. Data is taken from the European Environment Agency[1].

1.2 Thermoelectric Generators

Heat, for example, is an abundant and often wasted source of energy that is produced during e.g. factory and automotive processes, or as a result of our own metabolism (body heat). Thermoelectric generators (TEGs) are devices that could be used to harvest this waste energy by converting it into electrical power. While TEGs cannot act as a primary source of energy, they have the potential to increase the energy efficiency by making use of waste heat that is otherwise lost by energetic processes.

TEGs are able to generate electrical power from heat because they are constructed with thermoelectric materials. When a thermoelectric material experiences a temperature gradient a phenomenon called the Seebeck effect occurs. The Seebeck effect generates an electrical potential difference in the thermoelectric material that can then be used to drive an electrical current.

1.3 Thermoelectric Plastics

Commonly used thermoelectric materials are based on inorganic alloys, operating at relatively high temperatures >250°C, making them viable for high temperature processes. However, the best performing material, bismuth telluride, is expensive because it is a rare earth mineral. On the other hand, plastic TEGs are an attractive alternative because they consist of earth-abundant elements (such as: oxygen, carbon, nitrogen, sulphur) and in addition, they are malleable, light-weight and offer cost-effective processing from solution or melt while displaying substantially high thermoelectric performance. Another advantage is the ability to tune their thermoelectric parameters and processability by exploiting the vast tool box of polymer chemistry.

Due to the limited thermal stability of polymer-based TEGs, the prospective use of plastic TEG will be to harvest energy from low/moderate heat sources such as factory pipes and chimneys. Perhaps the most promising application area for plastic TEGs is to power electronics in the growing market of “Internet of things” (IoT). IoT is defined as a network of physical devices, vehicles, home appliances, and other items embedded with electronics, software, and sensors etc. that can connect and exchange data between each other. (Figure 2) In particular smart fabrics connected to the IoT could benefit from autonomous power supply from our own body heat.

The ability to tune processability, mechanical, electrical and thermal properties of semi-conducting polymers is not only an advantage but also possess a challenge. The ability to tune

the semi-conducting material in terms of molecular weight, regioregularity and polymer constitution can lead to markedly different properties of the resulting material.

To further complicate this the semiconducting polymer must be doped to optimise the thermoelectric performance. The concentration of dopant often reaches several tens of mole percent before optimal thermoelectric properties are observed. This large amount of dopant can have a substantial impact on the micro- and nanostructure, which strongly alter the energetic landscape, and therefore also thermoelectric properties of the resulting material.

1.4 Aim and Scope

This thesis seeks to unravel the complex structure-property relationships with regard to the thermoelectric properties of doped polymer semiconductors. First, the processing and characterisation of the semiconducting polymer poly(3-hexylthiophene) (P3HT) doped sequentially with 2,3,5,6-tetrafluoro-7,7,8,8-tetracyanoquinodimethane (F4TCNQ) from the vapor phase is described. Different processing solvents was used to alter the degree of solid-state order of P3HT, to study the impact on the electrical conductivity of the resulting material. Secondly, the Seebeck coefficient was measured to evaluate how the solid-state order affect the power factor (PF) of F4TCNQ doped P3HT.

Figure 2. More and more devices are connected to each other to exchange information. Could we use plastic thermoelectric generators to power the *Internet of Things*?

Chapter 2

2.1 General Principles of Thermoelectrics

If an electric conductor or semiconductor is put in contact with a heat source in one end and cold source in one end an electrical potential is created between the two ends, this potential can be used to drive a current. The effect is called the Seebeck effect and was discovered in 1821 by Thomas J. Seebeck. The created potential (*i.e.* accumulation of charges) due to a temperature gradient $\Delta T = T_{hot} - T_{cold}$, arises due to diffusion of charges from the hot to the cold side of the material and give rise to a potential difference ΔV. The Seebeck coefficient is temperature-dependent $\alpha(T) = -dV/dT$ and can be regarded as the average entropy per charge carrier. For small changes in the temperature α(T) is almost constant and we obtain: $\alpha = -(\Delta V/\Delta T)$. The sign of α indicates the type of carriers, α < 0 for electrons (n-type semiconductors) and α > 0 for holes (p-type semiconductors). To compare the performance of different thermoelectric materials the dimensionless figure of merit ZT is used:

$$ZT = \frac{\alpha^2 \sigma}{\kappa} T \tag{1}$$

where α is the Seebeck coefficient, σ the electrical conductivity and κ the thermal conductivity at a given absolute temperature T. The thermal conductivity κ can be challenging to measure for polymers, therefore the power factor (PF) is often used to compare different materials.

$$PF = \alpha^2 \sigma \tag{2}$$

The thermoelectric parameters α, σ, and κ are closely interlinked and can vary with temperature, this complicates optimisation and usually requires a compromise. The Seebeck coefficient can be seen as a measure of the average entropy per charge carrier and usually decreases upon addition of charge carriers (*i.e.* doping).

The electrical conductivity is described by the product of charge carrier concentration *n* and the mobility of the charge carrier μ:

$$\sigma = qn\mu \tag{3}$$

where *q* is the charge of the carrier *i.e.* ±1.6 x 10^{-19} C for electrons and holes.
The electrical conductivity σ strongly depends on the mobility μ of charge carriers which can be linked to the nanostructure of a semiconductor. The electrical conductivity also increases with the number of charge carriers *n*, an increase in charge carrier concentration often lead to a simultaneous decrease of the Seebeck coefficient and therefore the optimisation requires a trade-off.

For the thermal conductivity, the contribution of κ are both from phonons and electrons, where the electronic part is related to the electrical conductivity by proportionality constant *L* the Lorentz number*:*

$$\kappa_{electronic} = L\sigma T \tag{4}$$

It is valid for metals and, with restrictions, for some heavily doped organic materials. However, materials with low electrical conductivity will have a negligible electronic contribution to the thermal conductivity. Therefore the thermal conductivity can be set equal to the phonon contribution, which for many polymeric materials are in the range of 0.1 to 0.5 W m^{-1} K^{-1}. If the electrical conductivity of the semiconducting polymer would reach high values of about ~100 S cm^{-1} the contribution from $\kappa_{electronic}$ would approach or exceed κ_{phonon} and must therefore be taken into account.

2.2 Design of a Thermoelectric Generator

To achieve a sufficient voltage output (~ 1V) in order to power electronic components, one single piece of thermoelectric material is not enough. The general design principle is to connect a series of so called legs to increase the power output (Figure 3, left). One thermoelectric element consist of two legs (one n-type and one p-type), which have dissimilar material with different Seebeck coefficients so that the resulting thermovoltage does not cancel out.

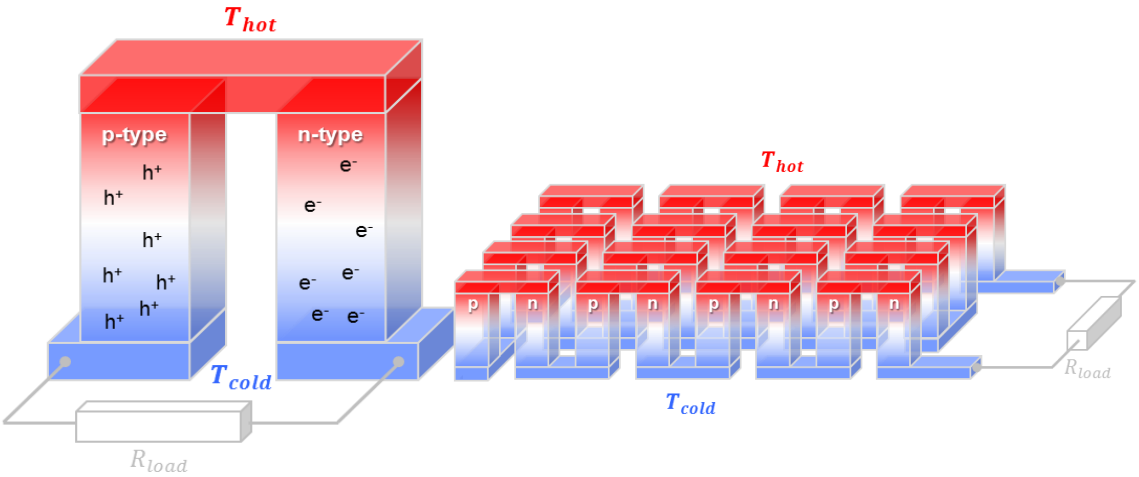

Figure 3. Schematics of a thermoelectric element (left), which comprises one n- and one p-type thermoelectric leg that experience a temperature gradient leading to charge accumulation at the cold ends, (right) a conventional thermoelectric module that comprises an array of elements, which are connected electrically in series but thermally in parallel. Reproduced with permission from ref. 2 – Published by The Royal Society of Chemistry.

These legs are then connected thermally in parallel but electrically in series (Figure 3, right) and the open circuit voltage V_{OC} can be presented as:

$$V_{OC} = N * (\alpha_1 - \alpha_2) * \Delta T \tag{5}$$

Where N is the number of elements, α is the different Seebeck coefficients (α_1 and α_2 having opposite signs). The maximum power P_{max} is gained when the external load and the internal resistance of the generator match, and is related to the V_{OC} according to:

$$P_{max} = \frac{{V_{OC}}^2}{4R_{internal}} \tag{6}$$

The power conversion efficiency (heat to electrical energy) η is given by $\eta = P/Q$ and increase with the figure of merit (ZT). As for all heat engines the efficiency is limited by the Carnot efficiency: $\eta_{carnot} = \Delta T/T_{hot}$ as well as internal losses as a result of Joule heating and heat conduction.

Alternative designs of thermoelectric legs might be needed since the n-type materials usually have a low stability in air. One option is to replace the n-type leg with a conductor with low Seebeck coefficient such as silver (*e.g.* $\alpha \sim 1.5\ \mu V\ K^{-1}$)[2]. Replacing the n-type legs with a regular conductor reduces P_{max} by a factor of about two, assuming that both V_{OC} and $R_{internal}$ are halved.

2.3 Conjugated Polymers

The Nobel Prize in chemistry 2000 was awarded jointly to Alan J. Heeger, Alan G. MacDiarmid and Hideki Shirakawa *"for the discovery and development of conductive polymers"*.[3] They discovered that polyacetylene could be made 10^9 times more conductive by oxidation (doping) with chlorine, bromine or iodine vapor (Figure 4). This sparked the interest for electrically conductive polymers.

A key property of conjugated polymers is their alternating single-double bond structure that gives rise to their semiconducting properties. The conjugated polymer feature sp^2 hybridised carbon atoms along the backbone whose p-orbitals become delocalised in π-orbitals. Due to energy level splitting, π and π^*-orbitals form a filled (highest occupied molecular orbital, HOMO) and an empty (lowest unoccupied molecular orbital, LUMO) conduction band with an energy gap in between. (Figure 5) The energy gap is called a bandgap E_g, and in a conjugated polymer the bandgap is much smaller than in saturated polymers. The smaller bandgap gives rise to their semiconducting nature and allows charge injection. However, conjugation is not enough to make the polymer electrically conductive. In addition charge carriers have to be injected, this process is called doping.

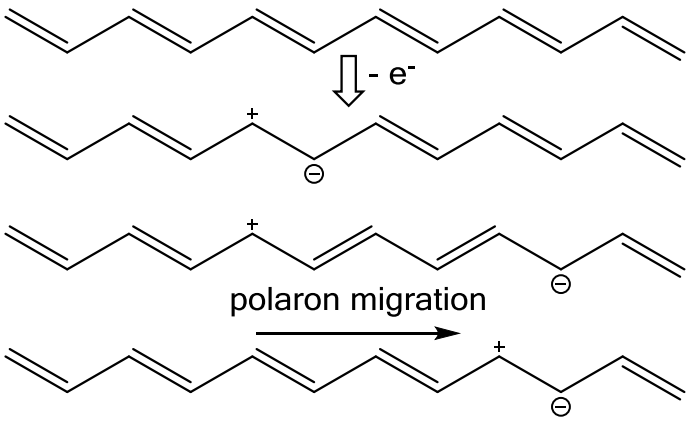

Figure 4. Schematic of polyacetylene doping and the radical cation ("polaron") formed by removal of one electron and (bottom) illustration of polaron migration.

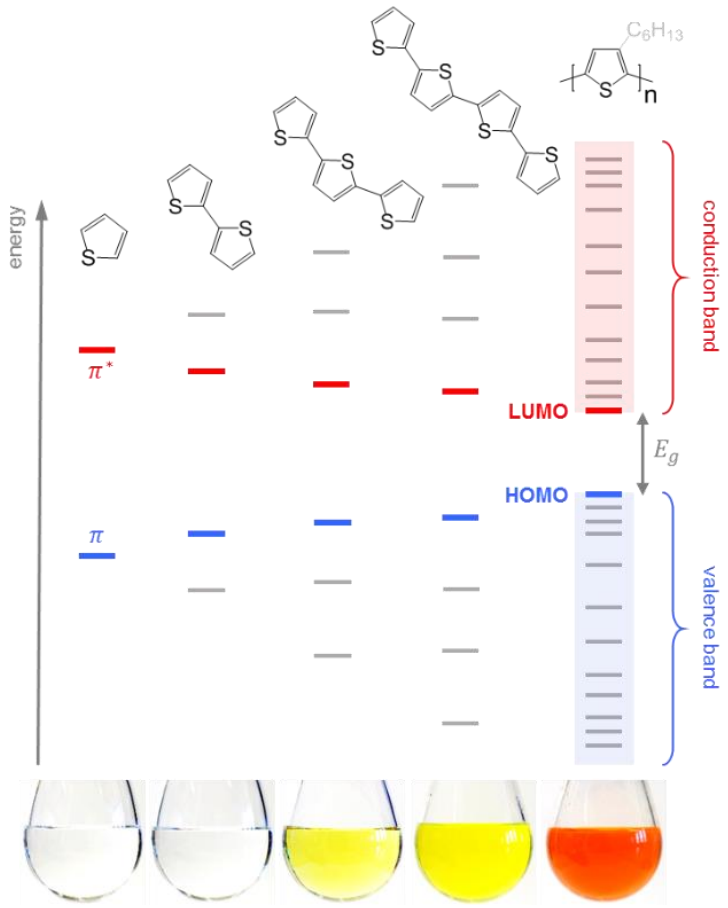

Figure 5. Evolution of the HOMO and LUMO levels as well as bandgap with increasing number of thiophene repeat units, resulting in valence and conduction bands for polythiophenes; the images of 5 g L^{-1} solutions in chloroform illustrate the narrowing of the bandgap, which leads to a red-shift in absorption for P3HT. Crystallisation as in spincoated thin films will lead to a further decrease in the bandgap due to electron delocalisation across adjacent chain segments. Reproduced with permission from ref. 2 – Published by The Royal Society of Chemistry.

2.4 Doping of Conjugated Polymers

The charge carrier concentration can be modulated through the addition of dopant. The dopant can either add or remove electrons from the polymer (n-type doping and p-type doping) (Figure 6), which introduces new electronic states (polarons or bipolarons) in the bandgap. Doping can be achieved in two ways (1) acid-base doping which refers to a transfer of a cation or anion to the polymer backbone or (2) redox doping, which refer to a transfer of electrons to form a donor-acceptor charge-transfer complex or ion-pair.

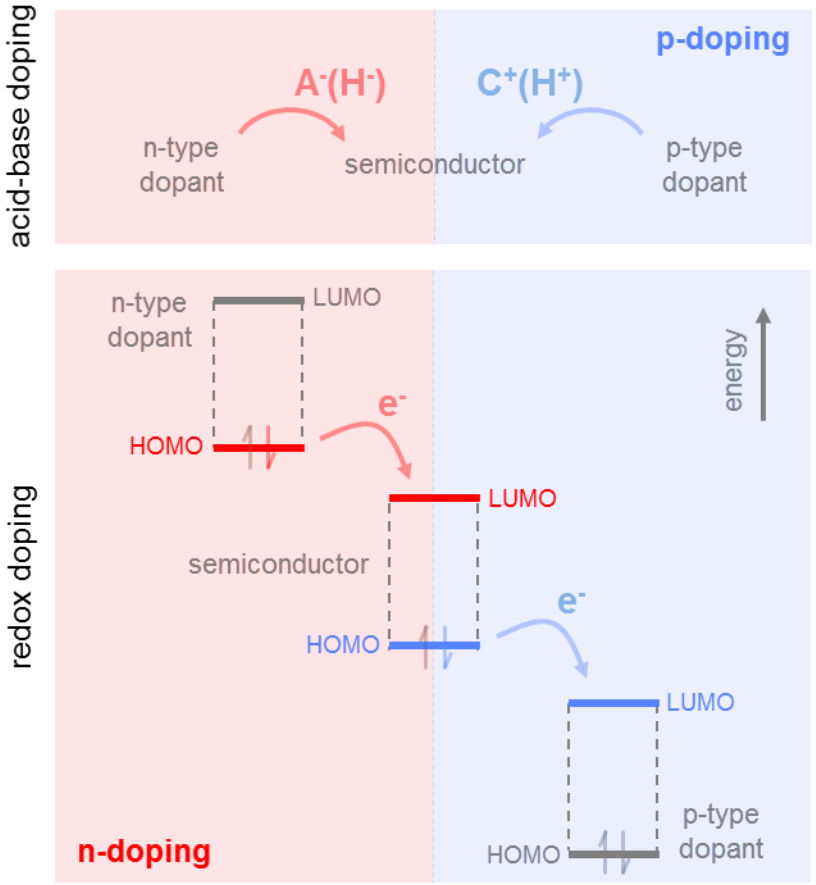

Figure 6. Basic principle of acid–base doping (top); and redox doping, which involves the transfer of an electron to the LUMO or from the HOMO of the semiconductor in the case of n- and p-doping, respectively (bottom). Reproduced with permission from ref. 2 – Published by The Royal Society of Chemistry.

2.5 Introduction of Dopant

The introduction of dopant to the polymer is a critical aspect to consider. Often the dopant concentration is in the order of several weight percent of the final material, therefore vast structural changes can be expected in the doped material compared to the neat material. Since changes in the nanostructure affect the charge transport it is important to know how these structural changes affect the material.

Generally two methods are used for doping (1) co-processing of the dopant and polymer in the same solution and (2) sequential doping where the polymer is allowed to solidify before the dopant is added either via an orthogonal solvent or via vapor.

2.6 P3HT Doped with F4TCNQ

A number of studies have focused on understanding the physics of charge transfer between P3HT and the p-type dopant F4TCNQ. It is established that integer charge transfer occurs from the HOMO (-4.8 eV) of P3HT to the LUMO of F4TCNQ (-5.2 eV).[4, 5]

Previous studies report vastly different numbers for the electrical conductivity of F4TCNQ-doped P3HT, ranging from 0.1 to 22 S cm^{-1} (Table 1). A comparison of the chosen processing protocols suggests that the best results are obtained when sequential processing is carried out. Sequential processing is thought to largely preserve the nanostructure of the P3HT film,[6-9] in contrast to when P3HT and F4TCNQ are co-processed from the same solution. Co-processing of the dopant and polymer form polymer:dopant ion pairs in the solution which disturb the solidification of P3HT leading to a poorly connected solid-state nanostructure, resulting in lower electrical conductivities. Currently, it is not known which polymer configuration (regioregularity, molecular weight) and nanostructure (degree of order) that should be selected to maximize the thermoelectric properties of P3HT doped with F4TCNQ.

Table 1. Highest reported values for the electrical conductivity σ_{max} of F4TCNQ-doped P3HT obtained through solution co-processing or sequential processing;

reference	σ_{max} (S cm^{-1})	method of doping
Yim *et al*. **2008**[10]	0.1	solution co-processing
Kiefer *et al.* **2017**[11]	0.1	solution co-processing
Glaudell *et al*. **2015**[12]	0.6	solution co-processing
Aziz *et al.* **2007**[13]	1.0	solution co-processing
Duong *et al*. **2013**[14]	1.8	solution co-processing
Jacobs *et al*. **2016**[6]	3.0	sequential processing (solution)
Kang *et al.* **2016**[7]	5.3	sequential processing (vapor)
Scholes *et al*. **2015**[8]	5.5	sequential processing (solution)
Jacobs *et al*. **2016**[6]	8.0	solution co-processing
Hamidi-Sakr *et al*. **2017**[9]	22.0[a]	sequential processing (solution)

[a] **σ_{max} along rubbing direction of aligned P3HT film (perpendicular $\sigma \sim 3$ S cm^{-1})**

Chapter 3

EXPERIMENTAL

3.1 Materials

Ten batches of P3HT (Table 2) were used in **paper 1**, for **paper 2** batch 7 was used. In both papers thin films of P3HT were doped with F4TCNQ from TCI Chemicals. For the processing, seven different solvents (purity > 99%) were used and were purchased from Sigma-Aldrich (o-dichlorobenzene, chlorobenzene, p-xylene, cyclohexanone, 1,2,4-trichlorobenzene) and Fisher Scientific (chloroform, toluene).

Table 2. Number- and weight-average molecular weight, M_n and M_w, regio-regularity rr, electrical conductivity of films spin-coated from CB/oDCB and vapor doped for t_{vapor} ~ 3min (2.5-5 min for batch 7), and source of the P3HT batches.

batch	M_n (kg mol^{-1})	M_w (kg mol^{-1})	rr (%)	σ (S cm^{-1})	source
1	16	45	28	0.01	Sigma Aldrich
2	27	73	84	2.0 ± 0.5	Solaris Chem Inc.
3	5	11	86	5.2 ± 0.6	Stingelin group
4	24	56	88	3.3 ± 0.7	Solaris Chem Inc.
5	56	127	95	2.9 ± 0.6	Stingelin group
6	9	19	96	4.3 ± 1.0	Ossila Ltd.
7	29	63	96	5.3 ± 2.1	Ossila Ltd.
8	64	106	95	3.2 ± 0.4	Sungyoung Ltd.
9	9	23	97	0.7 ± 0.1	Ossila Ltd.
10	12	30	97	2.8 ± 1.0	Merck KGaA

3.2 Sample Preparation

For both papers P3HT was dissolved at 60 °C at a concentration of 10 g L^{-1} in various solvents. For cyclohexanone the temperature was increased to 80 °C due to aggregation at lower temperatures. Thin films were spin-coated from hot solutions onto cleaned glass substrates. All solutions were spin-coated for 60 s at 1000 rpm, followed by 30 s at 3000 rpm to make sure the films were completely dry.

3.3 Vapor doping

In **paper 1** thermal gravimetric analysis (TGA) was used to study the evaporation rate of F4TCNQ at various temperatures. The temperature was kept constant at five different temperatures: 160, 170, 180, 190, and 200 °C for 2 and 10 h (180 °C) and the weight loss of ~ 3 mg of F4TCNQ was monitored. A doping temperature of 180 °C was chosen because of the high evaporation rate and at the same time moderate temperature to avoid degradation of the P3HT during doping. In **paper 1** and **paper 2** F4TCNQ was thermally evaporated onto P3HT thin films at ambient pressure using a home-built evaporation chamber (Figure 7) that consisted of a 15 × 20 mm large glass compartment in which films were suspended upside down, 10 mm above a crucible that contained ~20 mg of F4TCNQ. The crucible was heated to a temperature of 180 °C during doping on a hot plate, and a stainless-steel block was placed on top of the P3HT thin film to act as a heat sink to avoid thermal degradation of the polymer. The film temperature was measured with a hand-held temperature probe attached to the glass slide and reached a temperature of ~ 60 °C (3 min of doping).

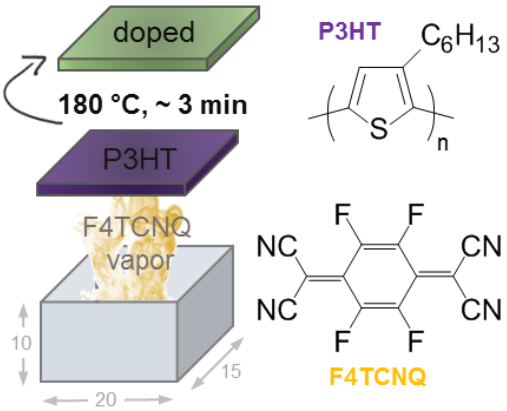

Figure 7. Schematic of home-built vapor doping chamber and chemical structures of P3HT and F4TCNQ.

3.4 Structural Characterisation

Grazing Incidence Wide-Angle X-ray Scattering (GIWAXS) was used in paper 1 to elucidate the structural order on the molecular length-scale by x-ray diffraction. The incoming beam is near horizontal to the sample surface in GIWAXS and is used when you want to probe the surface (or very thin films) of a sample.

3.5 Optoelectronic and Thermoelectric Characterisation

Ultraviolet Visible (UV-Vis) Absorption Spectroscopy

UV-vis spectroscopy is a technique that can measure electronic transitions in thin films of polymers. Polymers containing π-electrons or non-bonding electrons can absorb the energy in the form of light and excite these electrons to higher anti-bonding molecular orbitals. The more easily excited the electrons (i.e. lower energy gap between the HOMO and the LUMO), the longer the wavelength of light it can absorb. The light absorption spectrum can be determined measuring the absorption of light from high to low wavelength.

Electrical conductivity

The electrical conductivity is the ability of a material to transport charges. The electrical conductivity was measured with a four-point probe setup which has the advantage of eliminating possible contact resistance. A current is forced on the two outer electrodes and the voltage is measured on the two inner electrodes.

Seebeck coefficient

Seebeck coefficients are obtained by recording the voltage change when the material is subjected to a temperature gradient. Seebeck coefficients can be measured directly by measuring the voltage difference and maintaining a constant thermal gradient by two Peltier elements or it can be measured relatively by simultaneously subjecting the sample and a known reference (in our case Constantan) to the same thermal gradient. In the latter case there is an advantage that the exact temperature difference is not relevant as long as it is sufficiently low (~ 1 K). The change in voltage of the sample relative to the reference is proportional to the difference in Seebeck coefficient between the sample and reference.

3.6 Calculation of F4TCNQ Anion Concentration

To follow the doping of P3HT with F4TCNQ vapor UV-vis absorption spectra can be recorded. In the absorption spectra three different absorption bands are visible (1) neat F4TCNQ (390 nm), (2) neat P3HT (around 600 nm) and (3) F4TCNQ anions (410 and above 710 nm). The anion signal is increasing upon doping whilst the neat P3HT signal absorption is decreasing (Figure 8, left).

Figure 8 (right) shows a representative fit of an absorption spectra fitted as the sum of (I) the F4TCNQ anion signal, (II) two Gaussians corresponding to the polaronic absorption, and (III) a Gaussian model representing the absorption of P3HT aggregates. The extracted intensity of the F4TCNQ anion was then used to determine the F4TCNQ anion concentration (mol cm^{-3}) with the known extinction coefficient.[11, 18] Absorption spectra of neat P3HT were fitted according to refs [15-17] and absorption spectra of doped P3HT were fitted according to ref [18].

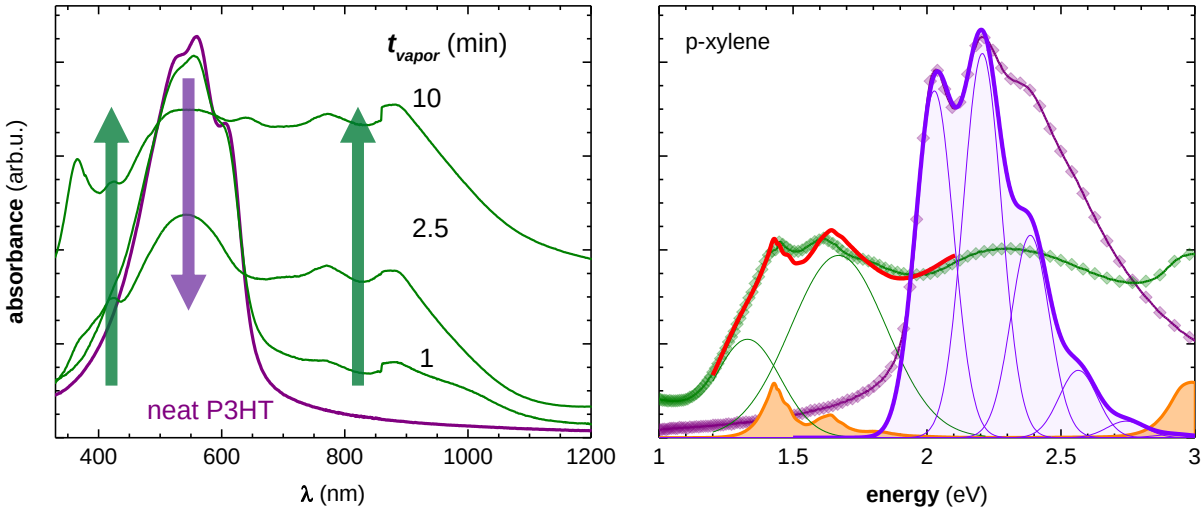

Figure 8. (Left) Representative absorption spectra of thin films of neat P3HT and doped for 1, 2.5 and 5 min and (right) fitted spectra of neat P3HT coated from p-xylene (purple), doped P3HT (green) and the F4TCNQ anion (orange).

Chapter 4

RESULTS

4.1 Elucidating Structure-Property Relationships of P3HT Doped with F4TCNQ Vapor (paper I)

The aim of this work is to investigate what properties of the semiconducting polymer P3HT are important to maximize the electrical conductivity of the doped polymer. P3HT with different regioregularity, molecular weight and varying degree of solid-state order was investigated with regard to the effect on electrical conductivity.

Vapor doping of P3HT

To be able to preserve the solid-state order in P3HT upon doping the polymer, vapor doping was chosen as the dopant method and the *calibration* of the set-up described in section 3.3. To ensure a high reproducibility we performed two extensive studies regarding to (1) doping time and (2) film thickness (Figure 9). We found that a doping time of 3 minutes gave us reproducible results regarding electrical conductivity and elimination of excess dopant on the surface that negatively affect the electrical conductivity. For the thickness study we found that samples with a thickness of up to 130 nm and a vapor doping time of ~ 3 min resulted in a comparable electrical conductivity. Therefore, in all subsequent experiments we chose to work with samples that were not more than 130 nm thick.

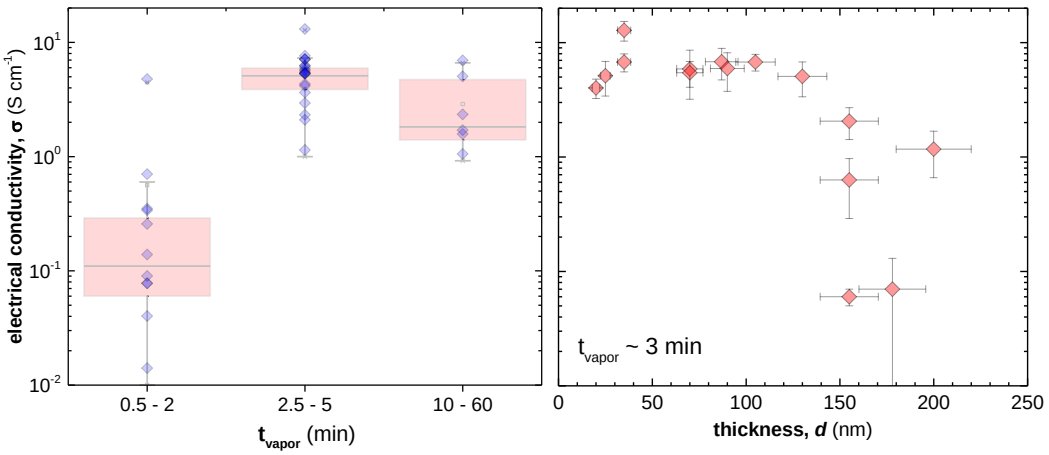

Figure 9. Electrical conductivity as a function of doping time (left) and as a function of thickness (right)

Solid-state structure of neat and vapor-doped films of P3HT

The impact of doping on the molecular packing of P3HT was evaluated using GIWAXS, for both neat and doped P3HT the majority of crystals indicate edge-on orientation (Figure 10). Upon doping the lamellar stacking distance shift from d_{100} = 1.59 to 1.91 nm and the π-stacking distance shift from d_{010} = 0.39 to 0.36 nm. The observed shifts are consistent with previous literature for P3HT doped with F4TCNQ [4, 8, 14] and indicate that the F4TCNQ is incorporated in the layer of hexyl side chains but does not disrupt the π-packing to a larger degree and therefore highly preserves the nanostructure of the polymer.

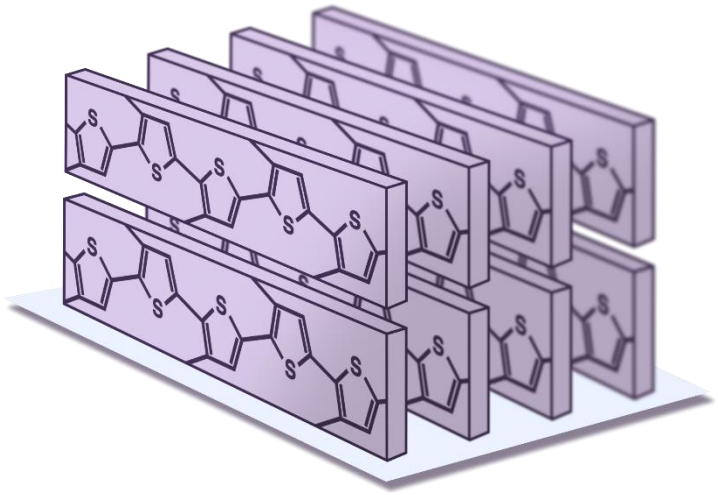

Figure 10. Edge-on orientation of a P3HT crystallite with the π-stacking direction lying in-plane to the surface.

Influence of regioregularity of P3HT upon doping with F4TCNQ

To investigate the impact of regioregularity on the doping and electrical conductivity we chose to work with four batches of P3HT with similar molecular weights but different regioregularity (between 28 (regiorandom) to 96 %). The doping of P3HT with F4TCNQ requires that the HOMO of the polymer is higher than the LUMO of the dopant for efficient charge transfer. We anticipated that lower regioregular P3HT would have a low driving force for electron transfer due to the lower lying HOMO, resulting in low doping levels.

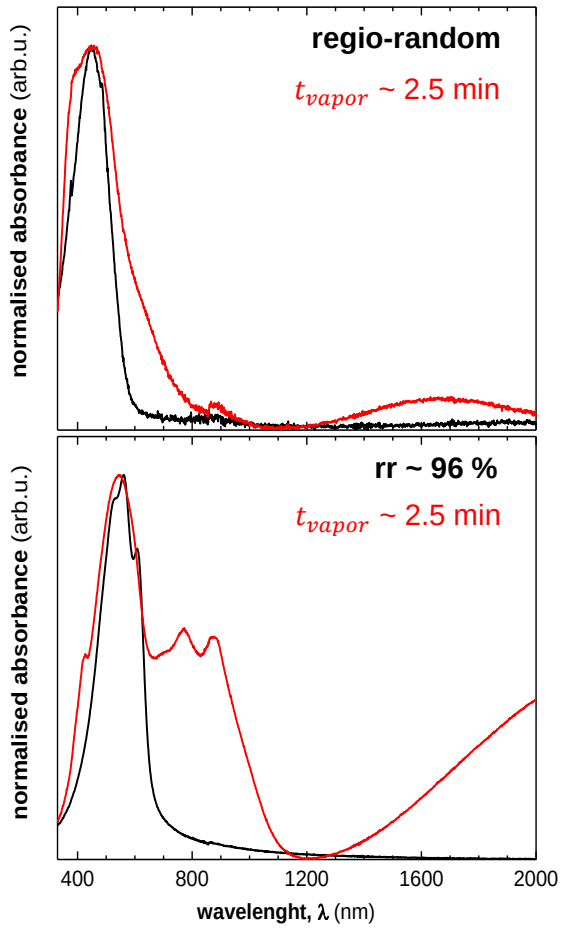

Figure 11. Normalised absorption spectra of regio-random P3HT (top) and 96 % regio-regular P3HT (bottom) spin coated from CB/oDCB, leading to an electrical conductivity of 0.01 and 6 S cm^{-1} respectively. Black line represents the neat P3HT and red line represents the doped P3HT.

As anticipated the regiorandom P3HT only showed low degree of doping validated with UV-vis spectroscopy (Figure 11, top) and resulted in an electrical conductivity of only 0.01 S cm^{-1}. P3HT with a regioregularity of < 84 % could readily be doped and the electrical conductivity increased with increasing regioregularity reaching ~ 6 S cm^{-1} for the highly regioregular P3HT (rr = 96 %) (Figure 11, bottom).

Interplay of P3HT solid-state order and electrical conductivity

It is well known that the degree of solid-state order strongly influences the charge transport in semiconducting polymers such as P3HT.[19-23] We therefore studied the influence of solid-state order of P3HT on the electrical conductivity of doped P3HT.

To vary the solid-state order we used a highly regioregular P3HT (rr ~ 96 %) and prepared thin films by spin-coating from seven different solvents: cyclohexanone, chloroform (CF), chlorobenzene (CB), chlorobenzene/ortho-dichlorobenzene (CB/oDCB), toluene, 1,2,4-trichlorobenzene (TCB) and p-xylene. By choosing solvents that are compatible with P3HT (e.g. dissolves the polymer) and that have dissimilar evaporation rate (e.g. time for the polymer to crystallise) one can obtain thin films of P3HT with varying solid-state order.

UV-vis absorption spectra was used to determine the degree of order in the thin film and was recorded prior to doping (Figure 12). From the recorded spectra the free exciton bandwidth *W* was extracted according to work by Spano *et.al.*[15-17] A decrease in the free exciton bandwidth *W* can be correlated to an increased aggregation and correlation length of P3HT.

Through analysis of the UV−vis spectra we calculated that the free exciton bandwidth, varied between 140 meV for cyclohexanone to 50 meV for p-xylene. Indicating an increased solid-state order for films coated from p-xylene. We went further to vapor dope the preformed thin films of P3HT with varying degree of solid-state order to see if we could correlate the order with the electrical conductivity of the doped samples. By plotting the electrical conductivity against the free exciton bandwidth *W* we could indeed see a correlation between the solid-state order of P3HT and electrical conductivity (Figure 13). Increasing the solid-state order of P3HT by coating from p-xylene resulted in an electrical conductivity of 12.7 S cm^{-1}.

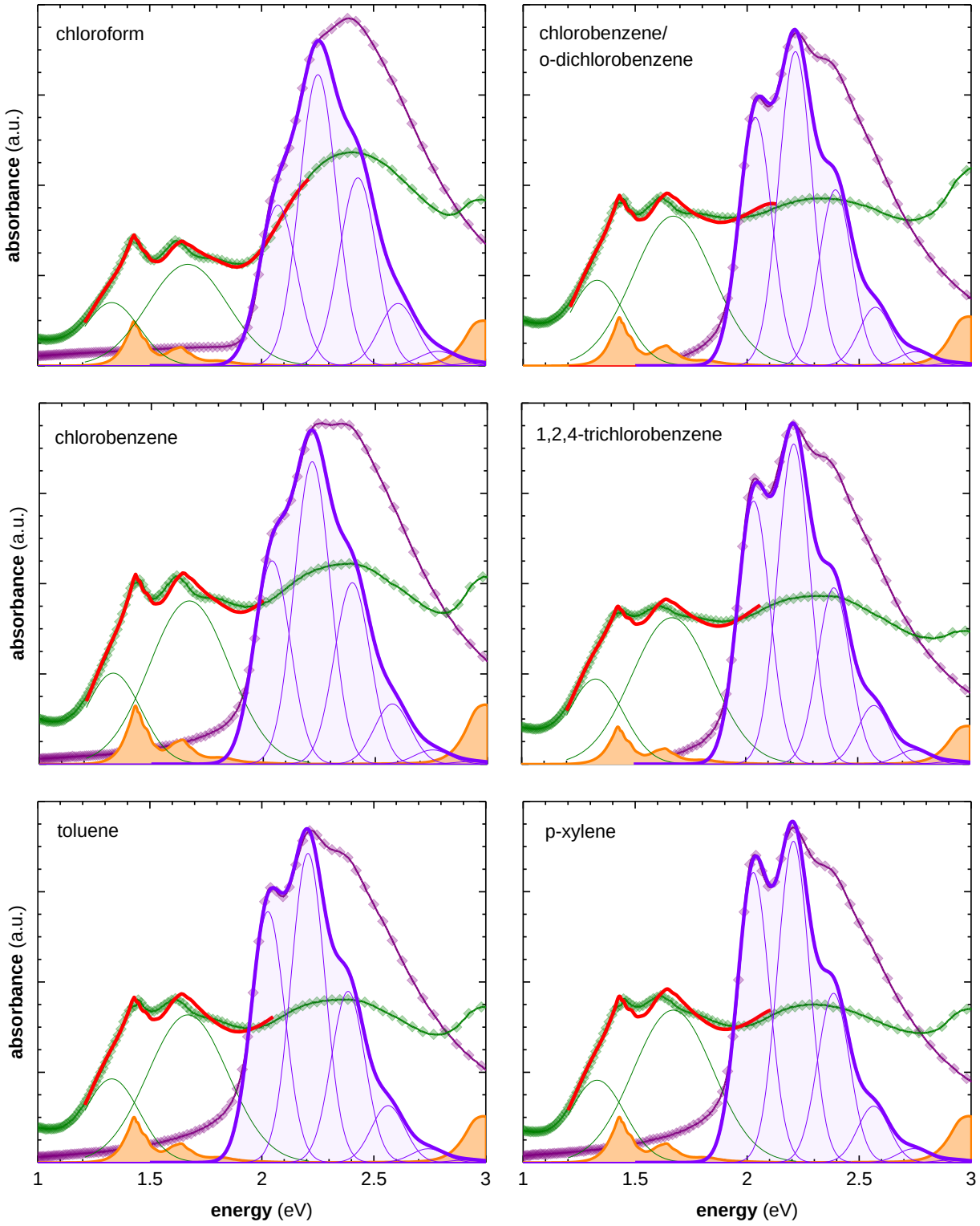

Figure 12. UV-vis absorption spectra of neat P3HT films spincoated from various solvents at 60 °C (purple symbols), and films vapor doped for 3 min (green symbols); spectra of neat P3HT are fitted according to ref [15-17]; spectra of doped P3HT and measured absorption spectrum of the F4TCNQ anion (orange) are fitted from ref [11, 18].

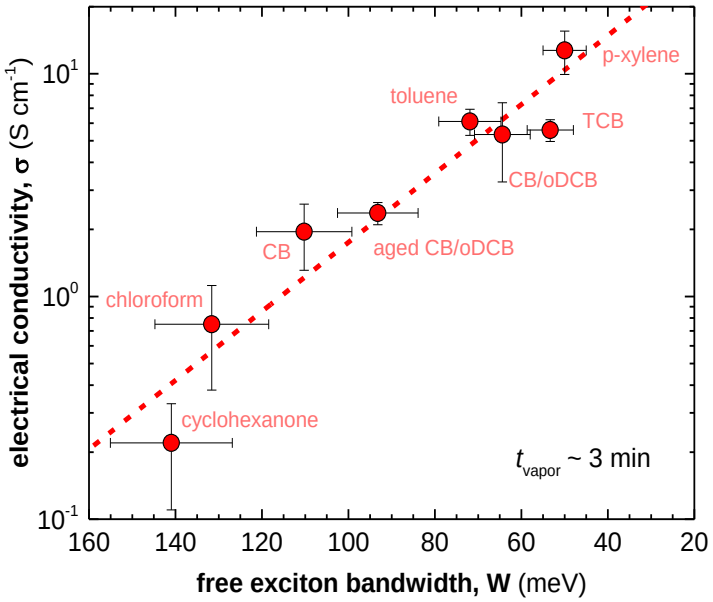

Figure 13. Electrical conductivity *σ* as a function of free exciton bandwidth *W* for P3HT spin coated from various solvents.

Interplay of molecular weight of P3HT and electrical conductivity

Another parameter that is well known to affect charge transport in neat P3HT is the molecular weight.[24] Two main effects need to be considered (1) the effect of chain entanglement on processing and solid-state nanostructure formation and (2) the effect of tie chains on charge transport. Chain entanglement in P3HT occurs at molecular weights of M_n > 25 kg mol^{-1},[24] and reduces crystallisation rate of P3HT during solution processing. High molecular weight P3HT can at the same time enhance the charge transport by bridging adjacent crystallites and aid charge carriers in traversing less conducting amorphous areas.[23]

To investigate the effect of molecular weight on the electrical conductivity of doped P3HT two series of P3HT were investigated (high vs low regioregular P3HT). Both series contained materials with a molecular weight considerable below and above the onset of entanglement and tie chain formation. We noticed that the electrical conductivity of doped P3HT did not vary with molecular weight (Figure 14). UV−vis spectra of P3HT batches with high regioregularity indicated that higher molecular weight samples are less ordered when spin-coated from CB/oDCB as compared to lower molecular weight batches.

We rationalised this decrease in order with the presence of chain entanglements that reduce the ability of the polymer to crystallise. Changing the processing solvent to p-xylene leads to a higher degree of solid-state order as seen previously and also an increase in electrical conductivity (Figure 14). For strongly doped P3HT, charge transport does not appear to suffer from an absence of connectivity between crystalline domains (through tie chains), which implies that the mechanical and electrical properties can be optimised independently.

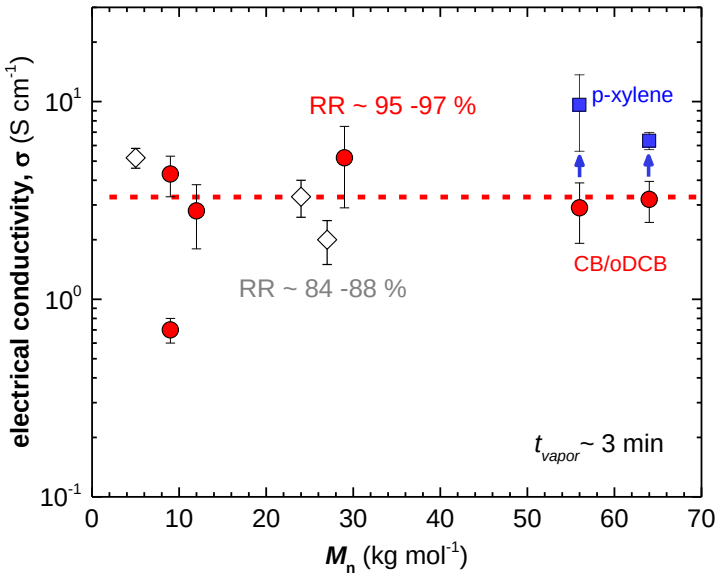

Figure 14. Electrical conductivity as a function of P3HT molecular weight: regio-regularity of (◊) 84-88% and (●) 95-97%; a change in processing solvent to p-xylene (■) increases the solid-state order and hence electrical conductivity of high-molecular weight P3HT.

F4TCNQ anions, charge-carrier density and average mobility

The reason for the increased electrical conductivity can be explained and motivated by equation (3). An increase in the degree of order may affect the number of charge carriers *n* and/or the mobility μ of charge carriers which in turn would lead to a change in the electrical conductivity. We estimated the concentration of F4TCNQ anions (Figure 12), for the majority of investigated samples we did not observe a difference in the number of F4TCNQ anions (1 to 4 x 10^{-4} mol cm^{-3}). Therefore the increase in electrical conductivity could be ascribed to an increase in charge carrier mobility due to an increased solid-state order of P3HT.

4.2 The Effect of Solid-state Order on the Thermoelectric Properties of Doped P3HT (paper 2)

The aim of this study was to investigate how the solid-state order of P3HT influences the Seebeck coefficient of the doped polymer. Together with the electrical conductivity measured in **paper 1** and the Seebeck data from **paper 2**, we calculated the power factor to see how/if the power factor varied with the solid-state order of P3HT.

The effect of solid-state order on the Seebeck coefficient

As discovered in **paper 1** the electrical conductivity scales with increasing solid-state order of P3HT, this increase in electrical conductivity can be attributed to the increased charge carrier mobility. In **paper 2** we measured the Seebeck coefficient for the same series of samples. For the most disordered films of P3HT coated from CF the Seebeck coefficient was measured to 51 μV K^{-1} and for the P3HT spin coated from p-xylene with highest degree of solid-state order we found a Seebeck coefficient of 46 μV K^{-1}.

For intermediate solid-state order (coated from CB, toluene, CB/oDCB and TCB) we found a Seebeck of ~ 60 μV K^{-1}. The Seebeck coefficient predominately probes mobile charge carriers and therefore a change in their concentration will influence the thermovoltage. In **paper 1** we investigated the concentration of F4TCNQ anions which did not vary between the samples. We therefore attribute the change in the Seebeck coefficient to the doping of different regions in the P3HT.

Doping of amorphous vs crystalline regions of P3HT

In our samples both disordered, amorphous and crystalline domains are present. Doping of crystalline domains readily leads to a free charge because the polymer is already planarised. A planar conformation facilitates delocalisation of hole charges.[25] Instead, in the amorphous regions the molecular motions are more restricted and therefore doping cannot induce the same degree of order that is already present in crystalline domains. This in turn would lead to that some charges are bound, leading to an increase in the Seebeck coefficient for less ordered samples of P3HT.

Mobility enhanced or mobility limited, a comparison of literature data

We made a comparison of our results with other reports for a number of different polythiophenes (Figure 15), to compare samples that are mobility enhanced vs mobility limited.

The variation of Seebeck coefficient with electrical conductivity follows the empirical trend $\alpha \propto \sigma^{-1/4}$ (dotted line, Figure 15).[12] Data points that lie to the left of this empirical trend are thought to be mobility limited. Mobility limited materials will have charges that cannot traverse the material sufficiently quickly because their motions are impeded by structural defects, as seen for the sample coated from CF.

The opposite case are samples that are mobility enhanced, where charges are able to traverse the material more quickly than predicted by the empirical trend. An example of mobility enhanced sample can be found in recent work by Brinkmann *et al.*, who studied sequentially-doped P3HT films that had been uniaxially aligned through rubbing.[9] Upon doping with F4TCNQ an increase in the electrical conductivity and Seebeck coefficient was observed, which can be rationalised with improved connectivity along the direction of orientation. We could conclude that our samples (except the film coated from CF) follow the empirical trend $\alpha \propto \sigma^{-1/4}$.

Power factor of vapor doped P3HT

By varying the degree of solid-state order of P3HT we could increase the thermoelectric power factor $\alpha^2\sigma$ from 0.2 to 2.7 μW m^{-1}. We ascribe this behaviour to improved charge-carrier mobility and hence electrical conductivity. In contrast we observed small changes in the Seebeck coefficient. This indicates that to improve the thermoelectric power factor of conjugated polymer based materials, we should primarily focus on enhancing the electrical conductivity of the material.

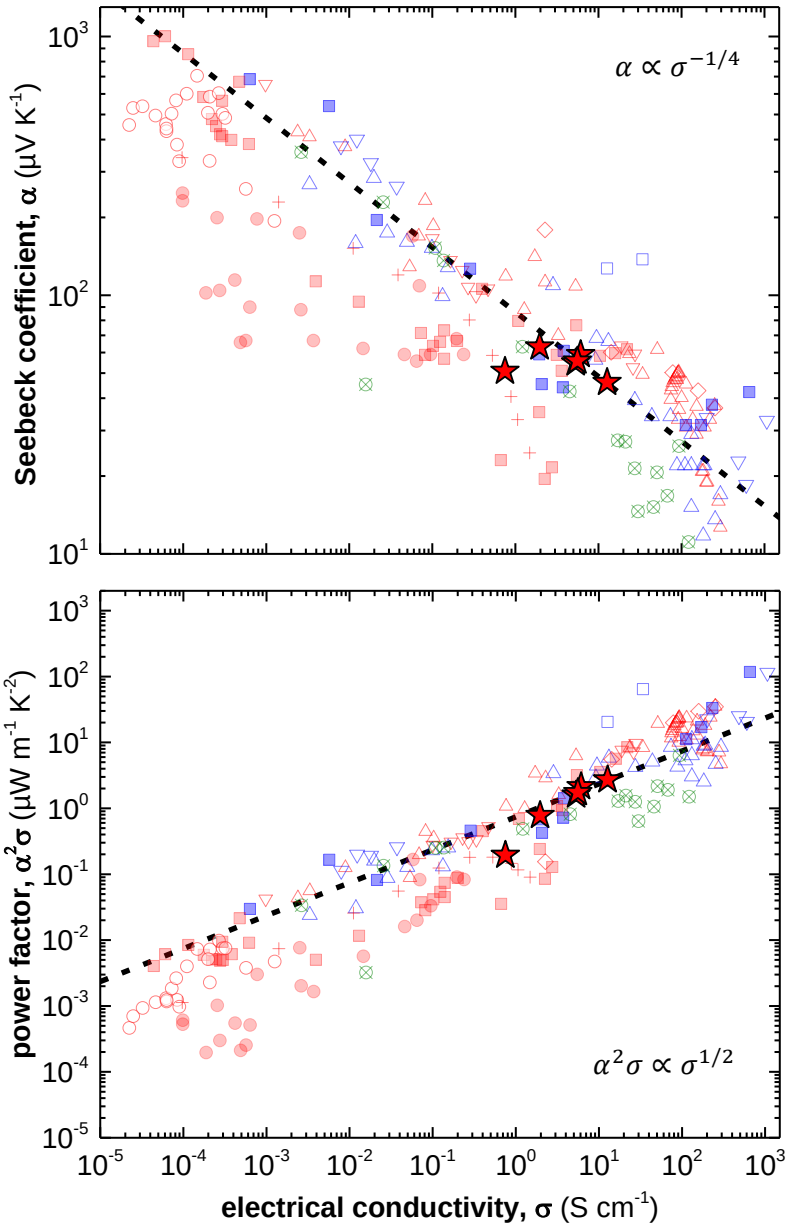

Figure 15. Seebeck coefficient (top) and power factor (bottom) as a function of electrical conductivity, data from paper 1 and paper 2 (red stars), and extracted from literature: P3HT doped with F4TCNQ (■),[12, 26-28] NOPF6 (┼),[29] FTS or TFSI (Δ),[12, 26-28] or FeCl3 (◊)[30]; P3HT:PEO doped with F4TCNQ (●)[11]; P3HT:P3HTT doped with F4TCNQ (○)[31]; PBTTT doped with F4TCNQ (■),[12, 32] FTS or TFSI (Δ),[12, 26, 33] or F2TCNQ (□)[32]; and p(g42T-T) doped with F4TCNQ or DDQ (¤).[34]

Chapter 5

CONCLUSION AND OUTLOOK

Conclusion

A robust vapor doping set-up was first established, where sequential doping of P3HT with F4TCNQ-vapor was performed. Moreover it was demonstrated how the effect of regioregularity, solid-state order and molecular weight of P3HT influenced the electrical conductivity.

Samples with a regioregularity of rr > 84% could readily be doped by F4TCNQ vapor. Regiorandom P3HT only showed a low degree of doping probed with UV-vis spectroscopy and led to an electrical conductivity of only 0.01 S cm^{-1}. The degree of solid-state order of P3HT strongly influenced the electrical conductivity of P3HT, leading to an electrical conductivity of 12.7 S cm^{-1}. The molecular weight of P3HT was varied between 5 to 64 kg mol^{-1} and did not strongly affect the electrical conductivity, which implies that for strongly doped P3HT the mechanical and electrical properties can be optimised independently.

Secondly, the thermoelectric power factor was evaluated and was found to increase with the solid-state order of P3HT from 0.2 to 2.7 μW m^{-1}. The variation in the Seebeck coefficient was found to be small varying between 46 to 59 μV K^{-1}. Therefore the improved power factor could be ascribed to improved charge-carrier mobility and hence electrical conductivity. To further improve the power factor of conjugated polymer based materials the focus should be on enhancing the electrical conductivity of these materials by selecting processing procedures that lead to a for charge transport beneficial solid state order.

Outlook

In future studies it would be interesting to further increase the solid-state order of P3HT by alignment methods such as rubbing or tensile-drawing, to investigate if we could achieve mobility enhanced materials. This could further increase the electrical conductivity and power factor of P3HT. For drawn samples it is anticipated that vapor doping might not be able to penetrate the more bulky sample that are needed to draw films of P3HT. Sequential doping from solution could be investigated as a method of doping for the more bulky samples.

F4TCNQ readily sublimes after deposition, therefore it is important to study the stability of the dopant. The sublimation is further increased by increasing temperatures, it is therefore of importance to study the thermal stability of F4TCNQ.

Finally a comparison of different semiconducting polymers could be made to validate if the observed trends are valid for other types of semiconducting polymers.

ACKNOWLEDGMENT

I would like to thank my supervisor Christian for being a great supervisor, always taking time to discuss and guide me when I feel lost at work.

Thanks to Mattias, David, Renee and Liyang for fruitful discussions and for always lending a helping hand when I need one. Cheers guys!

For the rest of my group and co-workers at floor 8, thanks for being who you are, I have the best colleagues! Special thanks Lotta, without you it would be chaos at floor 8…

Thanks to Mattias and Melinda for unconditional support and love.

Nina and Meiju, I would not have made it here without you!

BIBLIOGRAPHY

1. Total greenhouse gas emission trends and projections, https://www.eea.europa.eu/data-and-maps/indicators/greenhouse-gas-emission-trends-6/assessment-1).
2. R. Kroon, D. A. Mengistie, D. Kiefer, J. Hynynen, J. D. Ryan, L. Yu and C. Müller, *Chem. Soc. Rev.*, 2016, **45**, 6147-6164.
3. B. Nordén, The Nobel Prize in Chemistry, 2000: Conductive polymers, https://www.nobelprize.org/nobel_prizes/chemistry/laureates/2000/advanced-chemistryprize2000.pdf).
4. H. Méndez, G. Heimel, S. Winkler, J. Frisch, A. Opitz, K. Sauer, B. Wegner, M. Oehzelt, C. Röthel, S. Duhm, D. Többens, N. Koch and I. Salzmann, *Nat. Commun.*, 2015, **6**, 8560.
5. I. Salzmann, G. Heimel, M. Oehzelt, S. Winkler and N. Koch, *Acc. Chem. Res.*, 2016, **49**, 370-378.
6. I. E. Jacobs, E. W. Aasen, J. L. Oliveira, T. N. Fonseca, J. D. Roehling, J. Li, G. Zhang, M. P. Augustine, M. Mascal and A. J. Moule, *J. Mater. Chem. C*, 2016, **4**, 3454-3466.
7. K. Kang, S. Watanabe, K. Broch, A. Sepe, A. Brown, I. Nasrallah, M. Nikolka, Z. Fei, M. Heeney, D. Matsumoto, K. Marumoto, H. Tanaka, S.-i. Kuroda and H. Sirringhaus, *Nat Mater*, 2016, **15**, 896-902.
8. D. T. Scholes, S. A. Hawks, P. Y. Yee, H. Wu, J. R. Lindemuth, S. H. Tolbert and B. J. Schwartz, *J. Phys. Chem. Lett.*, 2015, **6**, 4786-4793.
9. A. Hamidi-Sakr, L. Biniek, J.-L. Bantignies, D. Maurin, L. Herrmann, N. Leclerc, P. Lévêque, V. Vijayakumar, N. Zimmermann and M. Brinkmann, *Adv. Funct. Mater.*, 2017, **27**, 1700173.
10. K. H. Yim, G. L. Whiting, C. E. Murphy, J. J. M. Halls, J. H. Burroughes, R. H. Friend and J. S. Kim, *Adv. Mater.*, 2008, **20**, 3319-3324.
11. D. Kiefer, L. Yu, E. Fransson, A. Gomez, D. Primetzhofer, A. Amassian, M. Campoy-Quiles and C. Müller, *Adv. Sci.*, 2017, **4**, 1600203.
12. A. M. Glaudell, J. E. Cochran, S. N. Patel and M. L. Chabinyc, *Adv. Energy Mater.*, 2015, **5**, 1401072.
13. E. F. Aziz, A. Vollmer, S. Eisebitt, W. Eberhardt, P. Pingel, D. Neher and N. Koch, *Adv. Mater.*, 2007, **19**, 3257-3260.
14. D. T. Duong, C. Wang, E. Antono, M. F. Toney and A. Salleo, *Org. Electron.*, 2013, **14**, 1330-1336.
15. J. Clark, J.-F. Chang, F. C. Spano, R. H. Friend and C. Silva, *Appl. Phys. Lett.*, 2009, **94**, 163306.
16. F. C. Spano, *J. Chem. Phys.*, 2005, **122**, 234701.
17. F. C. Spano, *Chem. Phys.*, 2006, **325**, 22-35.
18. C. Wang, D. T. Duong, K. Vandewal, J. Rivnay and A. Salleo, *Phys. Rev. B*, 2015, **91**, 085205.

19. C. Müller, *Chemistry of Materials*, 2015, **27**, 2740-2754.
20. E. J. W. Crossland, K. Tremel, F. Fischer, K. Rahimi, G. Reiter, U. Steiner and S. Ludwigs, *Advanced Materials*, 2012, **24**, 839-844.
21. I. McCulloch, M. Heeney, C. Bailey, K. Genevicius, I. MacDonald, M. Shkunov, D. Sparrowe, S. Tierney, R. Wagner, W. Zhang, M. L. Chabinyc, R. J. Kline, M. D. McGehee and M. F. Toney, *Nature Materials*, 2006, **5**, 328.
22. R. Noriega, J. Rivnay, K. Vandewal, F. P. V. Koch, N. Stingelin, P. Smith, M. F. Toney and A. Salleo, *Nature Materials*, 2013, **12**, 1038.
23. S. A. Mollinger, B. A. Krajina, R. Noriega, A. Salleo and A. J. Spakowitz, *ACS Macro Letters*, 2015, **4**, 708-712.
24. F. P. V. Koch, J. Rivnay, S. Foster, C. Müller, J. M. Downing, E. Buchaca-Domingo, P. Westacott, L. Yu, M. Yuan, M. Baklar, Z. Fei, C. Luscombe, M. A. McLachlan, M. Heeney, G. Rumbles, C. Silva, A. Salleo, J. Nelson, P. Smith and N. Stingelin, *Progress in Polymer Science*, 2013, **38**, 1978-1989.
25. J. Gao, E. T. Niles and J. K. Grey, *J. Phys. Chem. Lett.*, 2013, **4**, 2953−2957.
26. Q. Zhang, Y. Sun, W. Xu and D. Zhu, *Macromolecules*, 2014, **47**, 609-615.
27. S. Qu, Q. Yao, L. Wang, Z. Chen, K. Xu, H. Zeng, W. Shi, T. Zhang, C. Uher and L. Chen, *NPG Asia Mater*, 2016, **8**, e292.
28. Q. Zhang, Y. Sun, W. Xu and D. Zhu, *Energy Environ. Sci.*, 2012, **5**, 9639-9644.
29. Y. Xuan, X. Liu, S. Desbief, P. Leclère, M. Fahlman, R. Lazzaroni, M. Berggren, J. Cornil, D. Emin and X. Crispin, *Phys. Rev. B*, 2010, **82**, 115454.
30. C. T. Hong, Y. Yoo, Y. H. Kang, J. Ryu, S. Y. Cho and K.-S. Jang, *RSC Advances*, 2015, **5**, 11385-11391.
31. J. Sun, M. L. Yeh, B. J. Jung, B. Zhang, J. Feser, A. Majumdar and H. E. Katz, *Macromolecules*, 2010, **43**, 2897-2903.
32. S. N. Patel, A. M. Glaudell, K. A. Peterson, E. M. Thomas, K. A. O'Hara, E. Lim and M. L. Chabinyc, *Sci. Adv.*, 2017, **3**, e1700434.
33. S. N. Patel, A. M. Glaudell, D. Kiefer and M. L. Chabinyc, *ACS Macro Lett.*, 2016, **5**, 268-272.
34. R. Kroon, D. Kiefer, D. Stegerer, L. Y. Yu, M. Sommer and C. Müller, *Adv. Mater.*, 2017, **29**, 1700930.